

Scaling Laws Governing the Collapse of a Bose–Einstein Condensate

Sebastian J. Morris, Christopher J. Ho, Simon M. Fischer, Jiří Etrych,
Gevorg Martirosyan, Zoran Hadzibabic, and Christoph Eigen*

Cavendish Laboratory, University of Cambridge, J. J. Thomson Avenue, Cambridge CB3 0HE, United Kingdom

We study the collapse of an attractive Bose–Einstein condensate, where an unstable system evolves towards a singularity, by numerically solving the underlying cubic-quintic nonlinear Schrödinger equation. We find good agreement between our simulations and the atom-loss measurements with a ^{39}K condensate. Our simulations reveal an interplay of weak collapse and the propensity of the system to form a hotspot, and we uncover new scaling laws that govern this behavior. We also identify promising signatures of the theoretically predicted, but so far experimentally elusive, elastic three-body interactions.

Collapse of nonlinear systems is ubiquitous in nature, from the breaking of ocean waves [1, 2] to the gravitational collapse of stars [3]. When attractive forces overwhelm dispersive ones, systems evolve towards a singularity in finite time. In practice, dissipative processes typically become relevant as the singularity is approached, and can stabilize the system.

The same cubic nonlinear Schrödinger equation is at the heart of the theoretical description of a variety of collapse phenomena [4, 5], including self-focusing of light [6], collapse of Langmuir waves in plasmas [7–9], and white-caps on choppy water [1]. A key role is played by the dimensionality: lower-dimensional systems tend to feature soliton solutions [10], including the celebrated Townes soliton in 2D [11–13], whereas 3D systems predominantly exhibit collapse. For the 3D collapse, there is a rich variety of self-similar solutions that predict how a singularity is approached, including nonpeaked solutions [5] and the counterintuitive weak collapse [14–16], where a stronger attractive nonlinearity leads to less dissipation. In comparison, little is understood about the dynamics after the collapse [4, 5], with possibilities including further collapse events and the formation of a hotspot [16–23], where an emergent effective potential sustains a wave-action flux into a dissipation region in which the wave remains localized for a prolonged time.

Ultracold atoms provide powerful analog simulators of this nonlinear Schrödinger equation; the sign and the strength of the cubic nonlinearity can be tuned using Feshbach resonances [24], and inelastic three-body recombination naturally acts as a quintic dissipation mechanism. Collapse experiments have been performed with atomic Bose–Einstein condensates in harmonic [25–31] and box traps [32] (see also [33]), and both the criterion and the time for the collapse to occur have been understood. Moreover, by isolating single-collapse events, the weak nature of the 3D collapse was observed [32]. However, the scaling of the atom loss with the strengths of the cubic and quintic nonlinearities did not follow Zakharov’s analytic prediction [15], and was never fully understood.

In this Letter, we perform numerical simulations of collapse in the cubic-quintic nonlinear Schrödinger equation. Focusing on single-collapse events, the extracted total loss agrees with the measurements with a box-trapped ^{39}K Bose–Einstein condensate. The time-resolved loss dynamics feature an interplay of weak collapse and the propensity of the system to form a hotspot, and we uncover new scaling laws that govern this behavior. We also study the effects of the theoretically predicted, but experimentally elusive, elastic three-

body interactions [41–46]. At their predicted strength, these interactions modify the single-collapse loss only slightly, at a level that is not resolved in the experiments. However, we find promising signatures in the time-resolved loss dynamics, including significantly longer dissipation times and suppression of the hotspot behavior.

In dimensionless form, the nonlinear Schrödinger equation with an elastic cubic and dissipative quintic term reads:

$$i \frac{\partial \psi}{\partial t} = -\nabla^2 \psi + \alpha |\psi|^2 \psi - i\eta |\psi|^4 \psi, \quad (1)$$

where α and $\eta > 0$ are real. We initially ($t = 0$) normalize the wavefunction $\psi(r, t)$ to unity inside a spherical box of unit diameter and enforce the boundary condition $\psi = 0$ at the trap walls. To convert from dimensionless units to the experimental ones for the collapse of a box-trapped condensate [32], one rescales $r \rightarrow r/L$, $\psi \rightarrow L^{-3/2} \psi$, and $t \rightarrow t/\tau$, where L is the characteristic box size, $\tau = 2mL^2/\hbar$ the characteristic timescale, and m the atom mass, and uses

$$\alpha = \frac{8\pi a N_0}{L}, \quad \eta = \frac{N_0^2 m \mathcal{L}_3}{\hbar L^4}, \quad (2)$$

where a is the s -wave scattering length, N_0 the initial condensate atom number, and \mathcal{L}_3 the three-body loss coefficient.

Assuming $\eta = 0$ and a characteristic wavefunction extent ℓ in Eq. (1), the kinetic energy is $\propto 1/\ell^2$ and the interaction energy is $\propto \alpha/\ell^3$. As sketched in Fig. 1(a), for slightly negative α collapse is prevented by a kinetic energy barrier, which disappears at a negative critical value α_c .

As illustrated in Fig. 1(b), after α is quenched (at $t = 0$) from above to below α_c , the system approaches a singularity in time t_s . The density profile, $n(r, t) = |\psi(r, t)|^2$, is predicted [15], for $t \rightarrow t_s$, to evolve self-similarly with a peaked scaling solution χ :

$$n(r, t) = n_0(t) \chi[r/r_0(t)], \quad (3)$$

with $\chi(0) = 1$, $\chi \propto (r_0/r)^2$ for $r \gg r_0$, $r_0 \propto \sqrt{t_s - t}$, and $n_0(t) = n(0, t) \propto 1/|\alpha|(t_s - t)$. The collapse is termed *weak* because the fraction of the wave that is collapsing towards the origin, $n_0 r_0^3 \propto \sqrt{t_s - t}/|\alpha| \propto 1/\sqrt{n_0|\alpha|^3}$, diminishes as n_0 diverges, with stationary tails, $n(r) \propto 1/(|\alpha|r^2)$, left behind (see also [47]).

Introducing weak dissipation, $\eta \ll |\alpha|$, the quintic term in Eq. (1) significantly affects the dynamics once it becomes comparable to the cubic one, which happens for $n_0 \propto |\alpha|/\eta$ and corresponding $r_0 \propto \eta^{1/2}/|\alpha|$. At this point in time, the

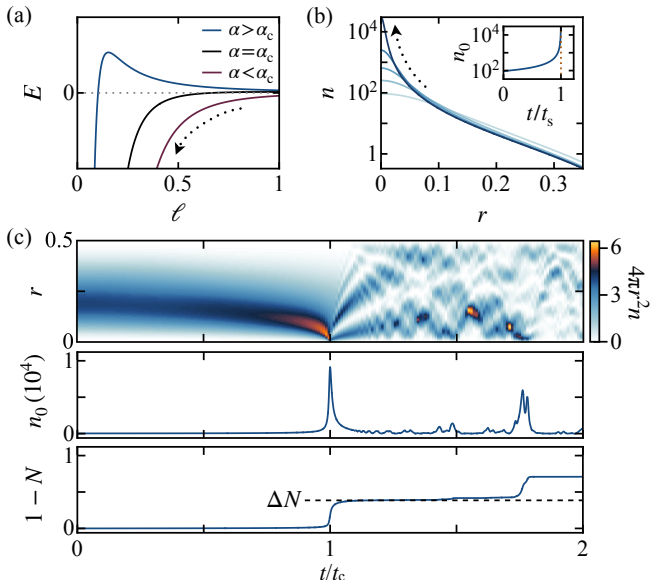


FIG. 1. Weak collapse. (a) Sketch of the effective energy landscape for a wavefunction of extent ℓ . The interaction energy is $\propto \alpha/\ell^3 < 0$ and collapse occurs (arrow) for $\alpha < \alpha_c$. (b) Typical evolution of the density profile $n(r, t)$ after a quench of α from above to below α_c . As the system approaches the singularity (light to dark colors), the central density diverges at a time t_s (see inset), and a diminishing fraction of the wave approaches the singularity, with stationary tails left behind. (c) Simulation results for a spherical box with $\alpha_c = -3.89(1)$, $\alpha = -4.2$, and nonzero dissipation strength $\eta = 3 \times 10^{-4}$ [see Eq. (1)]. We show the dynamics of the radial population density $4\pi r^2 n$ (top), the central density n_0 (middle), and the fractional loss $1 - N$ (bottom), where $N = \int 4\pi r^2 n dr \leq 1$; t_c is the time when n_0 first peaks (note that $t_c \rightarrow t_s$ for $\eta \rightarrow 0$ [48]). The dashed line indicates ΔN , the total single-collapse loss.

proportion of the wave that is still collapsing towards the origin is $\propto \eta^{1/2}/\alpha^2$. Assuming that this part is lost due to dissipation, while the tails are unaffected, gives the Zakharov scaling law for the fractional loss ΔN in a single-collapse event [7]:

$$\Delta N \propto \eta^{1/2}/\alpha^2, \quad (4)$$

which, counterintuitively, is smaller for a more unstable system (larger $|\alpha|$). These scaling arguments provide some intuition, but a complete understanding of collapse in Eq. (1) is lacking [5], and it is in general difficult to simulate due to the necessary spatiotemporal resolution [22, 49, 50].

Here, we assume spherical symmetry [51] and numerically solve the radial part of Eq. (1) in 1D (see [47] for details). We mimic the experimental protocol from Ref. [32] by starting from the metastable state for $\alpha = -3.6$, above $\alpha_c \approx -3.9$. We then quench to $\alpha < \alpha_c$, and record the evolution of ψ for different values of η .

In Fig. 1(c) we show a typical example of the simulated dynamics, which reveals an isolated first collapse event, followed by rich dynamics, including refocusing and subsequent collapses. We plot the evolution of the radial population density $4\pi r^2 n(r, t)$ (top), the central density n_0 (middle), and the loss $1 - N(t)$ (bottom), where $N(t) = \int 4\pi r^2 n(r, t) dr \leq 1$. Here t_c is the time when n_0 first peaks [48] and the dashed line shows the extracted ΔN ; note that throughout this Letter we focus on the first collapse event.

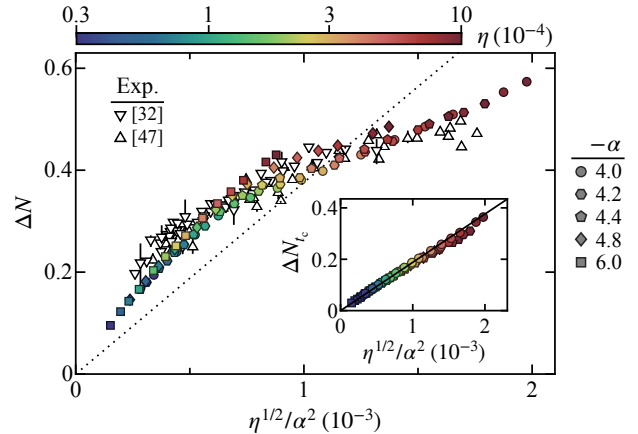


FIG. 2. Single-collapse atom-loss scaling laws. Plot of ΔN versus $\eta^{1/2}/\alpha^2$, comparing the experimental data (open triangles) to our simulations with different α (colored symbols) and η (color bar). The inset shows the simulated ΔN_{t_c} , the loss up to t_c , which follows the prediction in Eq. (4) (solid line), and suggests that the different scaling of ΔN arises due to dynamics in the aftermath of the singularity; the dotted line shows $\Delta N = 2\Delta N_{t_c}$. Note that the systematic uncertainty in experimentally determining $\eta^{1/2}/\alpha^2$ is $\pm 20\%$.

In Fig. 2, we compare our results for $\alpha \in [-4, -6]$ and $\eta \in [0.3, 10] \times 10^{-4}$ (colored symbols) to the measurements of ΔN with a box-trapped ^{39}K condensate [32, 47] (open triangles), finding good agreement. In both simulation and experiment, the data do not follow the prediction $\Delta N \propto \eta^{1/2}/\alpha^2$ [Eq. (4)]. However, as shown in the inset, the loss up to t_c , denoted ΔN_{t_c} , does show this scaling (solid line), so the difference must occur after t_c (cf. dotted line, which shows $\Delta N = 2\Delta N_{t_c}$).

To elucidate the collapse dynamics, we look at the time-resolved loss rate $\dot{N} = dN/dt = -8\pi\eta \int n^3 r^2 dr$. In Fig. 3(a), for $\alpha = -4.0$ and various η , we plot \dot{N}/\dot{N}_{\max} versus $(t - t_c)/t_d$, where \dot{N}_{\max} is the maximal instantaneous loss rate and t_d the dissipation time, defined as the full-width-half-maximum of $|\dot{N}(t)|$.

Before and near t_c , the curves coincide, meaning that $\Delta N_{t_c} \propto t_d |\dot{N}_{\max}|$. This is consistent with the Zakharov weak-collapse picture [22], with the characteristic size of the dissipation region $r_d \propto r_0(t_c) \propto \eta^{1/2}/|\alpha|$, density $n_d = n_0(t_c) \propto |\alpha|/\eta$, and time $t_d \propto \eta/\alpha^2$, such that $t_d |\dot{N}_{\max}| \propto t_d \eta n_d^3 r_d^3 \propto \eta^{1/2}/\alpha^2$, as in Eq. (4). We define r_d so that $n(r_d, t_c) = n_d/2$, and have verified the scaling laws for n_d , r_d , t_d , and \dot{N}_{\max} (see [47]).

However, for the smaller η values the loss extends to longer times, with a prominent ‘shoulder’ at $t > t_c$. As illustrated in the inset, the corresponding density profiles remain localized for much longer ($\gtrsim 5t_d$), which is a key signature of hotspot formation [16–23] (see also [55]).

In Fig. 3(b) we extend our analysis to different α values and show that the hotspot shoulder exhibits remarkably universal behavior: at a fixed $(t - t_c)/t_d > 0$, we empirically find that \dot{N}/\dot{N}_{\max} is a function of $\eta^{1/2}/|\alpha|^3$ [56]. To our knowledge, this scaling has not been predicted, and invites further study [57].

In Fig. 3(c) we introduce the loss asymmetry $A \equiv 2\Delta N_{t_c}/\Delta N - 1$, which is also a universal function of $\eta^{1/2}/|\alpha|^3$. Interestingly, in the regime where the hotspot behavior is

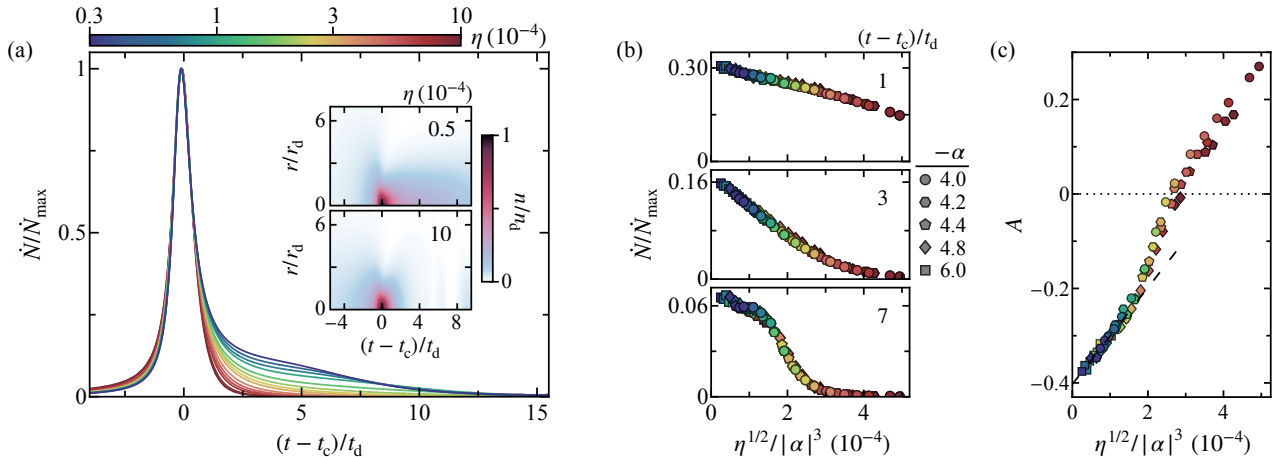


FIG. 3. Time-resolved loss dynamics revealing the scaling laws that govern the propensity to form a hotspot. (a) Normalized loss rate \dot{N}/\dot{N}_{\max} versus $(t - t_c)/t_d$ for $\alpha = -4.0$ and varying η ; here t_d is the full-width-half-maximum of $|\dot{N}(t)|$. For smaller η , the universal weak-collapse peak is accompanied by a growing ‘shoulder’ (for $t > t_c$). The insets show $n(r, t)$ for $\eta = 5 \times 10^{-5}$ (top) and $\eta = 10^{-3}$ (bottom), where for the smaller η the density remains high and localized for a prolonged time, a key signature of hotspot behavior; here $n_d = n(0, t_c)$ and r_d is defined so that $n(r_d, t_c) = n_d/2$. (b) Plotting \dot{N}/\dot{N}_{\max} at three characteristic $(t - t_c)/t_d > 0$ (panels) versus $\eta^{1/2}/|\alpha|^3$ for different α (legend) and η [colors, as in (a)] reveals remarkably universal behavior. (c) The loss asymmetry $A = 2\Delta N_{t_c}/\Delta N - 1$ also shows universal behavior in $\eta^{1/2}/|\alpha|^3$. For $\eta^{1/2}/|\alpha|^3 \rightarrow 0$ we find that A approaches ≈ -0.4 ; the dashed line shows a linear fit for $\eta^{1/2}/|\alpha|^3 < 1 \times 10^{-4}$.

most pronounced ($\eta^{1/2}/|\alpha|^3 \rightarrow 0$), A approaches ≈ -0.4 (rather than -1), so that $\Delta N \approx 3.3\Delta N_{t_c}$. Note that this recovers the Zakharov scaling $\Delta N \propto \eta^{1/2}/\alpha^2$, and since A grows linearly for small $\eta^{1/2}/|\alpha|^3$ (dashed line), the next-order correction to ΔN is $\propto \eta/|\alpha|^5$. For large $\eta^{1/2}/|\alpha|^3$, A exceeds 0 because a significant fraction of the wave is lost already before t_c .

In experimental units, our simulations predict a size of the dissipation region $r_d L \approx 1.9 \times (m\mathcal{L}_3/\hbar)^{1/2}/(8\pi|a|)$, a peak density $n_d N_0/L^3 \approx 0.72 \times 8\pi\hbar|a|/(m\mathcal{L}_3)$, and a dissipation time $t_d \tau \approx 25 \times m^2 \mathcal{L}_3/(32\pi^2 \hbar^2 a^2)$ [47]; note that these do not depend on either N_0 or L . For ^{39}K with $\mathcal{L}_3 = 1.3(5) \times 10^{-41} \text{m}^6 \text{s}^{-1}$ [58] at $a = -0.3a_0$ [59] (where a_0 is the Bohr radius), $r_d L \approx 0.4 \mu\text{m}$, $n_d N_0/L^3 \approx 4 \times 10^4 \mu\text{m}^{-3}$, and $t_d \tau \approx 2 \text{ms}$. By leveraging nondestructive imaging techniques [62–64] to monitor the same cloud as it collapses, or by preparing samples with a small N_0 uncertainty [65] (to minimize shot-to-shot variations in t_c) it should be possible to experimentally resolve the collapse dynamics.

Note that beyond-mean-field effects [68], which are not captured by Eq. (1), are expected to be negligible in the current ^{39}K experiments, since $\sqrt{(n_d N_0/L^3)|a|^3} \approx 10^{-4} (a/a_0)^2 \lesssim 3 \times 10^{-4}$. However, by increasing $|a|$ while keeping $\alpha \approx \alpha_c$, it should be possible to also probe these effects; e.g. using $a = -30a_0$ would offer a sizable $\sqrt{(n_d N_0/L^3)|a|^3} \approx 0.1$ at t_c .

In the final part of this Letter, we extend our simulations to include elastic three-body interactions [41–46], predicted to accompany the inelastic ones in atomic gases [45, 46], by adding a real quintic term $\kappa|\psi|^4\psi$ to Eq. (1), i.e. $-i\eta \rightarrow -i\eta + \kappa$. The strengths of the elastic and inelastic three-body interactions are, respectively, $\kappa = \text{Re}[D]N_0^2/L^4$ and $\eta = -\text{Im}[D]N_0^2/L^4$, where D is the complex three-body scattering hypervolume [44]. Near the zero crossing of a Feshbach resonance, $\text{Im}[D] = -\mathcal{L}_3 m/\hbar$ is nonuniversal (as it depends on details of the short-range interactions) but it can readily be measured, whereas the elastic three-body interactions have

been predicted to be universally set by the van-der-Waals interaction length r_{vdW} , with $\text{Re}[D] \approx 100r_{\text{vdW}}^4$ [45, 46]. Combining this prediction with the independently measured

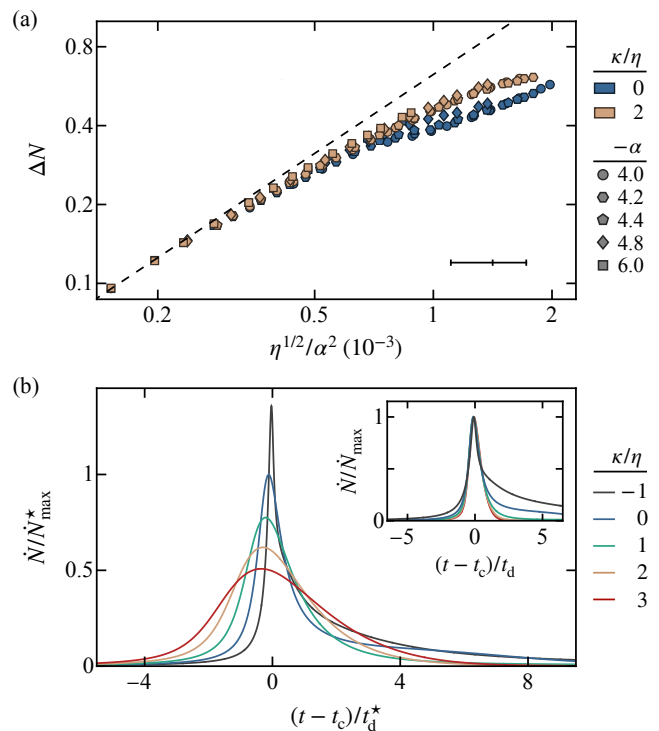


FIG. 4. Effects of elastic three-body interactions. (a) Plot of ΔN versus $\eta^{1/2}/\alpha^2$ for $\kappa/\eta = 2$ and $\kappa = 0$ (colors) on log-log scale, also varying both α (symbols) and $\eta \in [0.3, 10] \times 10^{-4}$ as in Fig. 2. For reference, the dashed line shows $\propto \eta^{1/2}/\alpha^2$, and the x error bar in the bottom right corner indicates the $\pm 20\%$ systematic uncertainty in experimentally determining $\eta^{1/2}/\alpha^2$ [66]. (b) Time-resolved \dot{N} for different κ/η (legend) and fixed $\alpha = -4.4$ and $\eta = 10^{-4}$, highlighting that the dissipation time t_d and hotspot behavior are highly sensitive to κ/η , even though the differences in ΔN are small. The main panel shows \dot{N}/\dot{N}_{\max}^* versus $(t - t_c)/t_d^*$, where the stars (*) indicate $\kappa = 0$ values, while the inset shows individually normalized curves.

$-\text{Im}[D] = 60(20)r_{\text{vdW}}^4$ for ^{39}K [58] suggests $\kappa/\eta \approx 2$.

In Fig. 4(a) we show ΔN versus $\eta^{1/2}/\alpha^2$ for both $\kappa/\eta = 2$ and $\kappa = 0$ on log-log scale, with the same α and η values as in Fig. 2. The differences in ΔN between the two are relatively small ($\lesssim 20\%$), and moreover, cannot be resolved within the systematic uncertainty of $\pm 20\%$ in experimentally determining $\eta^{1/2}/\alpha^2$.

However, as illustrated in Fig. 4(b) for $\eta^{1/2}/\alpha^2 \approx 5 \times 10^{-4}$ ($\alpha = -4.4$ and $\eta = 10^{-4}$), the time-resolved loss dynamics are very sensitive to κ . For increasing κ , the time t_d increases, \dot{N}_{max} decreases, and the hotspot behavior is suppressed. Note that, when $\kappa > 0$, the elastic three-body term plays a similar role to the dissipative one in slowing down the approach to the singularity (see [47] for additional details).

Experimental studies of the collapse dynamics in ^{39}K could thus offer a setting for observing elastic three-body interactions. To study the hotspot behavior, one could instead use other atoms with access to smaller predicted κ/η , e.g. for ^7Li with $-\text{Im}[D] \approx 5000r_{\text{vdW}}^4$ [69] one has $\kappa/\eta \approx 0.02$.

In conclusion, we numerically investigated collapse in the 3D cubic-quintic nonlinear Schrödinger equation, finding good agreement between our simulations and experiments performed with attractive box-trapped Bose–Einstein condensates. We demonstrated the propensity of the system to form a hotspot, uncovering new scaling laws that extend the Zakharov picture of weak collapse, and showed that collapse dynamics can be a sensitive probe of elastic three-body interactions. In the future, it would be interesting to further study the interplay between elastic and inelastic three-body interactions, for instance in the formation of quantum droplets [45, 46, 70–72]. It would also be interesting to study how the presence of a harmonic trap modifies the collapse dynamics, where soliton formation can play a role [28] and delayed collapses have been predicted [73]. More generally, studying collapse dynamics of other quantum fluids, including quantum mixtures [74] and dipolar condensates [75, 76], could offer more insights into the interactions governing their behavior (see e.g. [77–80]).

ACKNOWLEDGEMENTS

We thank Wilhelm Zwerger, Robert P. Smith, Martin Gazo, and Servaas Kokkelmans for discussions and comments on the manuscript. This work was supported by EP-SRC [Grant No. EP/P009565/1], ERC [UniFlat], and STFC [Grant No. ST/T006056/1]. Z.H. acknowledges support from the Royal Society Wolfson Fellowship.

* ce330@cam.ac.uk

- [1] A. Davey and K. Stewartson, On three-dimensional packets of surface waves, *Proc. R. Soc. Lond. A* **338**, 101 (1974).
- [2] M. L. McAllister, S. Draycott, R. Calvert, T. Davey, F. Dias, and T. S. van den Bremer, Three-dimensional wave breaking, *Nature* **633**, 601 (2024).
- [3] R. Penrose, Gravitational Collapse and Space-Time Singularities, *Phys. Rev. Lett.* **14**, 57 (1965).

- [4] C. Sulem and P.-L. Sulem, *The Nonlinear Schrödinger Equation: Self-Focusing and Wave Collapse* (Springer-Verlag, New York, 1999).
- [5] G. Fibich, *The Nonlinear Schrödinger Equation* (Springer International Publishing, Switzerland, 2015).
- [6] R. W. Boyd and S. G. Lukishova and Y. R. Shen (Eds.), *Self-focusing: Past and Present* (Springer Science & Business Media, New York, 2009).
- [7] V. E. Zakharov, Collapse of Langmuir Waves, *Sov. Phys. JETP* **35**, 908 (1972).
- [8] H. C. Kim, R. L. Stenzel, and A. Y. Wong, Development of "Cavitons" and Trapping of rf Field, *Phys. Rev. Lett.* **33**, 886 (1974).
- [9] A. Y. Wong and P. Y. Cheung, Three-Dimensional Self-Collapse of Langmuir Waves, *Phys. Rev. Lett.* **52**, 1222 (1984).
- [10] A. Scott, F. Chu, and D. McLaughlin, The soliton: A new concept in applied science, *Proc. IEEE* **61**, 1443 (1973).
- [11] K. D. Moll, A. L. Gaeta, and G. Fibich, Self-Similar Optical Wave Collapse: Observation of the Townes Profile, *Phys. Rev. Lett.* **90**, 203902 (2003).
- [12] C.-A. Chen and C.-L. Hung, Observation of Universal Quench Dynamics and Townes Soliton Formation from Modulational Instability in Two-Dimensional Bose Gases, *Phys. Rev. Lett.* **125**, 250401 (2020).
- [13] B. Bakkali-Hassani, C. Maury, Y.-Q. Zou, E. Le Cerf, R. Saint-Jalm, P. C. M. Castilho, S. Nascimbene, J. Dalibard, and J. Beugnon, Realization of a Townes Soliton in a Two-Component Planar Bose Gas, *Phys. Rev. Lett.* **127**, 023603 (2021).
- [14] V. E. Zakharov and V. S. Synakh, The nature of the self-focusing singularity, *Sov. Phys. JETP* **41**, 465 (1975).
- [15] V. E. Zakharov and E. A. Kuznetsov, A Quasi-Classical Theory for a Three-Dimensional Wave Collapse, *Sov. Phys. JETP* **64**, 773 (1986).
- [16] V. E. Zakharov and E. A. Kuznetsov, Solitons and collapses: two evolution scenarios of nonlinear wave systems, *Phys.-Usp.* **55**, 535 (2012).
- [17] V. E. Zakharov and L. N. Shur, Self-similar regimes of wave collapse, *Sov. Phys. JETP* **54**, 1064 (1981).
- [18] V. M. Malkin, Bi-self-similar wave collapse, *JETP Lett.* **48**, 603 (1988).
- [19] S. N. Vlasov, L. V. Piskunova, and V. I. Talanov, Three-dimensional wave collapse in the nonlinear Schrödinger equation model, *Sov. Phys. JETP* **68**, 1125 (1989).
- [20] V. E. Zakharov, N. E. Kosmatov, and V. F. Shvets, Ultrastrong wave collapse, *JETP Lett.* **49**, 431 (1989).
- [21] V. M. Malkin and E. G. Shapiro, Singular wave collapse, *Sov. Phys. JETP* **70**, 102 (1990).
- [22] N. Kosmatov, V. Shvets, and V. Zakharov, Computer simulation of wave collapses in the nonlinear Schrödinger equation, *Phys. D: Nonlinear Phenom.* **52**, 16 (1991).
- [23] B. J. LeMesurier, Dissipation at singularities of the nonlinear Schrödinger equation through limits of regularisations, *Phys. D: Nonlinear Phenom.* **138**, 334 (2000).
- [24] C. Chin, R. Grimm, P. Julienne, and E. Tiesinga, Feshbach resonances in ultracold gases, *Rev. Mod. Phys.* **82**, 1225 (2010).
- [25] J. M. Gerton, D. Strekalov, I. Prodan, and R. G. Hulet, Direct observation of growth and collapse of a Bose–Einstein condensate with attractive interactions, *Nature* **408**, 692 (2000).
- [26] J. L. Roberts, N. R. Claussen, S. L. Cornish, E. A. Donley, E. A. Cornell, and C. E. Wieman, Controlled Collapse of a Bose–Einstein Condensate, *Phys. Rev. Lett.* **86**, 4211 (2001).
- [27] E. A. Donley, N. R. Claussen, S. L. Cornish, J. L. Roberts, E. A. Cornell, and C. E. Wieman, Dynamics of collapsing and exploding Bose–Einstein condensates, *Nature* **412**, 295 (2001).
- [28] S. L. Cornish, S. T. Thompson, and C. E. Wieman, Formation of Bright Matter-Wave Solitons during the Collapse of Attractive Bose–Einstein Condensates, *Phys. Rev. Lett.* **96**, 170401 (2006).

- (2006).
- [29] P. A. Altin, G. R. Dennis, G. D. McDonald, D. Döring, J. E. Debs, J. D. Close, C. M. Savage, and N. P. Robins, Collapse and three-body loss in a ^{85}Rb Bose–Einstein condensate, *Phys. Rev. A* **84**, 033632 (2011).
- [30] R. L. Compton, Y.-J. Lin, K. Jiménez-García, J. V. Porto, and I. B. Spielman, Dynamically slowed collapse of a Bose–Einstein condensate with attractive interactions, *Phys. Rev. A* **86**, 063601 (2012).
- [31] Y. Huang, S. Nagata, J. Jachinowski, J. Hu, and C. Chin, Two dimensional arrays of Bose–Einstein condensates: interference and stochastic collapse dynamics, arXiv:2404.14142 (2024).
- [32] C. Eigen, A. L. Gaunt, A. Suleymanzade, N. Navon, Z. Hadzibabic, and R. P. Smith, Observation of Weak Collapse in a Bose–Einstein Condensate, *Phys. Rev. X* **6**, 041058 (2016).
- [33] While here we consider single-component Bose–Einstein condensates with contact interactions, related experiments have also been performed using dipolar gases [34–36], Bose–Bose mixtures [37, 38], and Bose–Fermi mixtures [39, 40].
- [34] T. Lahaye, J. Metz, B. Fröhlich, T. Koch, M. Meister, A. Griesmaier, T. Pfau, H. Saito, Y. Kawaguchi, and M. Ueda, d -Wave Collapse and Explosion of a Dipolar Bose–Einstein Condensate, *Phys. Rev. Lett.* **101**, 080401 (2008).
- [35] T. Koch, T. Lahaye, J. Metz, B. Fröhlich, A. Griesmaier, and T. Pfau, Stabilizing a purely dipolar quantum gas against collapse, *Nat. Phys.* **4**, 218 (2008).
- [36] H. Kadau, M. Schmitt, M. Wenzel, C. Wink, T. Maier, I. Ferrier-Barbut, and T. Pfau, Observing the Rosensweig instability of a quantum ferrofluid, *Nature* **530**, 194 (2016).
- [37] C. R. Cabrera, L. Tanzi, J. Sanz, B. Naylor, P. Thomas, P. Cheiney, and L. Tarruell, Quantum liquid droplets in a mixture of Bose–Einstein condensates, *Science* **359**, 301 (2018).
- [38] G. Semeghini, G. Ferioli, L. Masi, C. Mazzinghi, L. Wolswijk, F. Minardi, M. Modugno, G. Modugno, M. Inguscio, and M. Fattori, Self-Bound Quantum Droplets of Atomic Mixtures in Free Space, *Phys. Rev. Lett.* **120**, 235301 (2018).
- [39] G. Modugno, G. Roati, F. Riboli, F. Ferlaino, R. J. Brecha, and M. Inguscio, Collapse of a Degenerate Fermi Gas, *Science* **297**, 2240 (2002).
- [40] C. Ospelkaus, S. Ospelkaus, K. Sengstock, and K. Bongs, Interaction-Driven Dynamics of ^{40}K - ^{87}Rb Fermion-Boson Gas Mixtures in the Large-Particle-Number Limit, *Phys. Rev. Lett.* **96**, 020401 (2006).
- [41] T. T. Wu, Ground State of a Bose System of Hard Spheres, *Phys. Rev.* **115**, 1390 (1959).
- [42] Braaten, E. and Nieto, A., Quantum corrections to the energy density of a homogeneous Bose gas, *Eur. Phys. J. B* **11**, 143 (1999).
- [43] E. Braaten and H.-W. Hammer, Universality in few-body systems with large scattering length, *Phys. Rep.* **428**, 259 (2006).
- [44] S. Tan, Three-boson problem at low energy and implications for dilute Bose–Einstein condensates, *Phys. Rev. A* **78**, 013636 (2008).
- [45] W. Zwerger, Quantum-unbinding near a zero temperature liquid–gas transition, *J. Stat. Mech.* **2019**, 103104 (2019).
- [46] P. M. A. Mestrom, V. E. Colussi, T. Secker, G. P. Groeneveld, and S. J. J. M. F. Kokkelmans, van der Waals Universality near a Quantum Tricritical Point, *Phys. Rev. Lett.* **124**, 143401 (2020).
- [47] Supplemental Material including details on the form of the collapsing wavefunction, our numerical simulations, new experimental data, the accessible parameter range, and the Zakharov scaling laws.
- [48] In the Zakharov weak-collapse picture, when the collapsing part of the wave is lost at a time \tilde{t} , $n_0 \propto |\alpha|/\eta \propto 1/|\alpha|(t_s - \tilde{t})$, such that $(t_s - \tilde{t}) \propto \eta/\alpha^2 > 0$. In our simulations, we find that n_0 first peaks at a time $t_c > t_s$, because some dissipation occurs already before \tilde{t} and slows down the growth of n_0 .
- [49] B. J. LeMesurier, G. Papanicolaou, C. Sulem, and P. L. Sulem, Focusing and multi-focusing solutions of the nonlinear Schrödinger equation, *Phys. D: Nonlinear Phenom.* **31**, 78 (1988).
- [50] W. Bao and Y. Cai, Mathematical theory and numerical methods for Bose–Einstein condensation, *Kinet. Relat. Models* **6**, 1 (2013).
- [51] Studies of the symmetric collapse solution to Eq. (1) with $\eta = 0$ have shown stability against azimuthal perturbations [19]. We expect this assumption to break down for large quenches below α_c , where the amplification of local instabilities plays a significant role [12, 52, 53] (see also [5, 54]).
- [52] J. K. Chin, J. M. Vogels, and W. Ketterle, Amplification of Local Instabilities in a Bose–Einstein Condensate with Attractive Interactions, *Phys. Rev. Lett.* **90**, 160405 (2003).
- [53] S. Banerjee, K. Zhou, S. K. Tiwari, H. Tamura, R. Li, P. Kevrekidis, S. I. Mistakidis, V. Walther, and C.-L. Hung, Collapse of a quantum vortex in an attractive two-dimensional Bose gas, arXiv:2406.00863 (2024).
- [54] V. I. Bespalov and V. I. Talanov, Filamentary Structure of Light Beams in Nonlinear Liquids, *JETP Lett.* **3**, 471 (1966).
- [55] Note that the hotspot behavior, which occurs for a single collapse event, is distinct from previously observed prolonged dissipation [27, 29, 32], which occurred due to multiple experimentally unresolved collapse events [32].
- [56] This also explains the weak breakdown of universality in the simulated ΔN in Fig. 2 (most visible for $\eta^{1/2}/\alpha^2 \approx 10^{-3}$, where larger $|\alpha|$ values give slightly larger ΔN).
- [57] Although previous analytical studies of the d -dimensional cubic nonlinear Schrödinger equation have identified ‘quasi-stationary’ dissipative solutions with a singularity at the origin for $d \geq 3$ [18–21], numerical simulations have only shown hotspots unambiguously for $d \geq 4$ [22, 23]. The hotspot behavior in the marginal $d = 3$ case is still not analytically understood.
- [58] M. Fattori, C. D’Errico, G. Roati, M. Zaccanti, M. Jonas-Lasinio, M. Modugno, M. Inguscio, and G. Modugno, Atom Interferometry with a Weakly Interacting Bose–Einstein Condensate, *Phys. Rev. Lett.* **100**, 080405 (2008).
- [59] For ^{39}K in the hyperfine ground state, the shallow zero-crossing at 350.4(1) G allows a to be finely tuned (with $0.02a_0$ precision). In the experiments we use $|a| \ll r_{\text{vdW}} = 64.6a_0$ [60], for which one expects \mathcal{L}_3 not to vary significantly (see e.g. [61]).
- [60] S. Falke, H. Knöckel, J. Friebe, M. Riedmann, E. Tiemann, and C. Lisdat, Potassium ground-state scattering parameters and Born–Oppenheimer potentials from molecular spectroscopy, *Phys. Rev. A* **78**, 012503 (2008).
- [61] Y. Wang and P. S. Julienne, Universal van der Waals physics for three cold atoms near Feshbach resonances, *Nat. Phys.* **10**, 768 (2014).
- [62] M. R. Andrews, M.-O. Mewes, N. J. van Druten, D. S. Durfee, D. M. Kurn, and W. Ketterle, Direct, Nondestructive Observation of a Bose Condensate, *Science* **273**, 84 (1996).
- [63] R. Meppelink, R. A. Rozendaal, S. B. Koller, J. M. Vogels, and P. van der Straten, Thermodynamics of Bose–Einstein-condensed clouds using phase-contrast imaging, *Phys. Rev. A* **81**, 053632 (2010).
- [64] M. Gajdacz, P. L. Pedersen, T. Mørch, A. J. Hilliard, J. Arlt, and J. F. Sherson, Non-destructive Faraday imaging of dynamically controlled ultracold atoms, *Rev. Sci. Instr.* **84**, 083105 (2013).
- [65] M. Gajdacz, A. J. Hilliard, M. A. Kristensen, P. L. Pedersen, C. Klempt, J. J. Arlt, and J. F. Sherson, Preparation of ultracold atom clouds at the shot noise level, *Phys. Rev. Lett.* **117**, 073604 (2016).
- [66] Note that for $\alpha = -4.0$, $\kappa/\eta = 2$, and our two largest η values, collapse does not occur, because increasing κ also reduces

- α_c [67]; we numerically obtain $\alpha_c \approx -3.89 - 40\kappa$.
- [67] F. K. Abdullaev, A. Gammal, L. Tomio, and T. Frederico, Stability of trapped Bose-Einstein condensates, *Phys. Rev. A* **63**, 043604 (2001).
 - [68] T. D. Lee and C. N. Yang, Many-Body Problem in Quantum Mechanics and Quantum Statistical Mechanics, *Phys. Rev.* **105**, 1119 (1957).
 - [69] Z. Shotan, O. Machtey, S. Kokkelmans, and L. Khaykovich, Three-Body Recombination at Vanishing Scattering Lengths in an Ultracold Bose Gas, *Phys. Rev. Lett.* **113**, 053202 (2014).
 - [70] A. Bulgac, Dilute quantum droplets, *Phys. Rev. Lett.* **89**, 050402 (2002).
 - [71] D. T. Son, M. Stephanov, and H.-U. Yee, Fate of multiparticle resonances: From Q-balls to ^3He droplets, *Phys. Rev. A* **106**, L050801 (2022).
 - [72] J. Hofmann, Corrections to reaction-diffusion dynamics above the upper critical dimension, *Phys. Rev. E* **105**, 024127 (2022).
 - [73] A. F. Biasi, J. Mas, and A. Paredes, Delayed collapses of Bose-Einstein condensates in relation to anti-de Sitter gravity, *Phys. Rev. E* **95**, 032216 (2017).
 - [74] C. Baroni, G. Lamporesi, and M. Zaccanti, Quantum mixtures of ultracold gases of neutral atoms, *Nat. Rev. Phys.* **6**, 736 (2024).
 - [75] L. Chomaz, I. Ferrier-Barbut, F. Ferlaino, B. Laburthe-Tolra, B. L. Lev, and T. Pfau, Dipolar physics: a review of experiments with magnetic quantum gases, *Rep. Prog. Phys.* **86**, 026401 (2022).
 - [76] N. Bigagli, W. Yuan, S. Zhang, B. Bulatovic, T. Karman, I. Stevenson, and S. Will, Observation of Bose-Einstein condensation of dipolar molecules, *Nature* **631**, 289 (2024).
 - [77] D. S. Petrov, Three-Body Interacting Bosons in Free Space, *Phys. Rev. Lett.* **112**, 103201 (2014).
 - [78] D. S. Petrov, Quantum Mechanical Stabilization of a Collapsing Bose-Bose Mixture, *Phys. Rev. Lett.* **115**, 155302 (2015).
 - [79] P. B. Blakie, Properties of a dipolar condensate with three-body interactions, *Phys. Rev. A* **93**, 033644 (2016).
 - [80] W. Zwerger, Reflections on dipolar quantum fluids, *arXiv:2411.02017* (2024).
 - [81] S. K. Adhikari and P. Muruganandam, Bose-Einstein condensation dynamics from the numerical solution of the Gross-Pitaevskii equation, *J. Phys. B: At. Mol. Opt. Phys.* **35**, 2831 (2002).
 - [82] P. Valero-Lara, I. Martínez-Pérez, R. Sirvent, X. Martorell, and A. J. Peña, cuThomasBatch and cuThomasVBatch, CUDA routines to compute batch of tridiagonal systems on NVIDIA GPUs, *Concurr. Comput. Pract. Exp.* **30**, e4909 (2018).

SUPPLEMENTAL MATERIAL

I. THE COLLAPSING WAVEFUNCTION

In Fig. S1(a), we show the evolution of the density profile $n(r, t)$ on log-log scale following a collapse-inducing quench to $\alpha = -4$ for $\eta \approx 0$, illustrating the weak-collapse picture.

In Fig. S1(b), we summarize the dynamics of $n(r)$ near t_c , for both $-5 < (t - t_c)/t_d < 0$ (top) and $0 < (t - t_c)/t_d < 5$ (bottom), and our set of $\alpha \in [-4, -6]$ and $\eta \in [0.3, 10] \times 10^{-4}$ values. Plotting n_0 versus $1/(\alpha r_0^2)$, where $r_0(t)$ is defined so that $n(r_0, t) = n_0/2$, shows that the relation between n_0 and r_0 is universal both before and after t_c .

In Fig. S1(c), for the same times as shown in Fig. S1(b), we plot all the normalized density profiles $n(r/r_0, t)/n_0(t)$, showing that for $r \lesssim 2r_0$ they are well captured by the same shape. Note that here $\gtrsim 95\%$ of the instantaneous loss takes place at $r < 2r_0$.

II. NUMERICAL SIMULATIONS

We solve Eq. (1) on a GeForce RTX 4070 GPU by assuming spherical symmetry and applying the time-splitting finite-difference method [50, 81], where we make use of the algorithm from Ref. [82] to solve the relevant tri-diagonal matrix systems.

We discretize space inside the unit-diameter box into 2^{12}

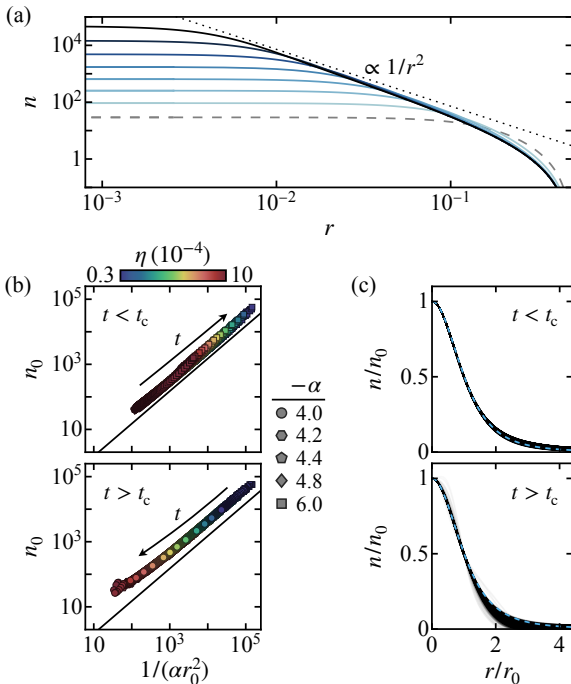


FIG. S1. Self-similar wavefunction evolution throughout the collapse. (a) Log-log plot of $n(r)$ at different times $t < t_c$ (light to dark colors), for $\alpha = -4$ and $\eta \approx 0$. The gray dashed line shows $n(r, 0)$. (b) Plot of n_0 versus $1/(\alpha r_0^2)$ for all our α (legend) and η (color bar), evenly sampled from $-5 < (t - t_c)/t_d < 0$ (top) and $0 < (t - t_c)/t_d < 5$ (bottom), revealing a universal scaling trajectory. For reference, the solid lines show $n_0 \propto 1/(\alpha r_0^2)$. (c) Plot of all the normalized density profiles $n(r/r_0, t)/n_0(t)$ for the same α , η , and t as shown in (b). Each individual curve is shown with 3% opacity and the dashed lines show squared Lorentzians.

evenly spaced radii from $r = 10^{-14}$ (to avoid divide-by-zero errors) to $r = 0.5$, with the boundary condition $\psi(0.5, t) = 0$ applied during each timestep $\Delta t \approx 1.5 \times 10^{-8}$. We have verified that varying both the spatial and/or temporal sampling by a factor 2 does not meaningfully affect our results.

III. NEW EXPERIMENTAL DATA

We perform additional measurements of ΔN as in Ref. [32], extending the range of $\eta^{1/2}/\alpha^2$ to larger values. We start with a quasipure ^{39}K Bose-Einstein condensate consisting of N_0 atoms in the lowest hyperfine state, confined in a cylindrical optical-box trap of radius R and length $L \approx 2R$, and tune the magnetic field to near the zero crossing at 350.4(1) G [58]. Note that we always use the $1/N_0$ -dependence of the critical interaction strength a_c to define the effective $a = 0$ [26, 32]. To initiate collapse, we quench a from above to below a_c , and measure ΔN .

In Fig. S2 we plot ΔN versus $\eta^{1/2}/\alpha^2$ (cf. Fig. 2), delineating the new data (blue circles and green diamonds) from previous measurements [32] (black triangles). Note that for the blue circles we quench from $\alpha \approx 0$ (instead of starting close to α_c [32]), demonstrating that ΔN is robust to the initial condition. The ΔN measurements span $\alpha \in [-4, -11]$ and $\eta \in [0.4, 15] \times 10^{-3}$. The key limitation for measuring ΔN for smaller $\eta^{1/2}/\alpha^2$ is the onset of multiple-collapse behavior [32], while reaching larger $\eta^{1/2}/\alpha^2$ is complicated by three-body loss becoming relevant already for $t \ll t_c$ and also during sample preparation.

IV. ZAKHAROV SCALING LAWS

In Fig. S3, we separately test the predictions for the different Zakharov weak-collapse scaling laws for n_d , r_d , t_d , and \dot{N}_{max} . The solid lines show linear fits to data with small dissipation ($\Delta N_{t_c} < 0.2$ corresponding to $\eta^{1/2}/\alpha^2 < 1.06 \times 10^{-4}$), yielding: $n_d \approx 0.72 \times |\alpha|/\eta$, $r_d \approx 1.9 \times \eta^{1/2}/|\alpha|$, $t_d \approx 25 \times \eta/\alpha^2$, and $|\dot{N}_{\text{max}}| \approx 4.1 \times \eta r_d^3 n_d^3 \approx 11/\eta^{1/2}$.

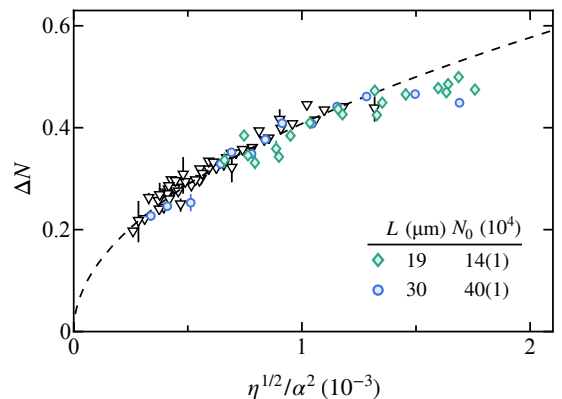


FIG. S2. New single-collapse loss measurements with ^{39}K . Plot of ΔN versus $\eta^{1/2}/\alpha^2$, showing the previous measurements from Ref. [32] (black triangles) alongside our new measurements (legend) that extend to larger values of $\eta^{1/2}/\alpha^2$. For reference, the dashed line shows $\Delta N \approx 13 \times \eta^{1/4}/|\alpha|$ [32].

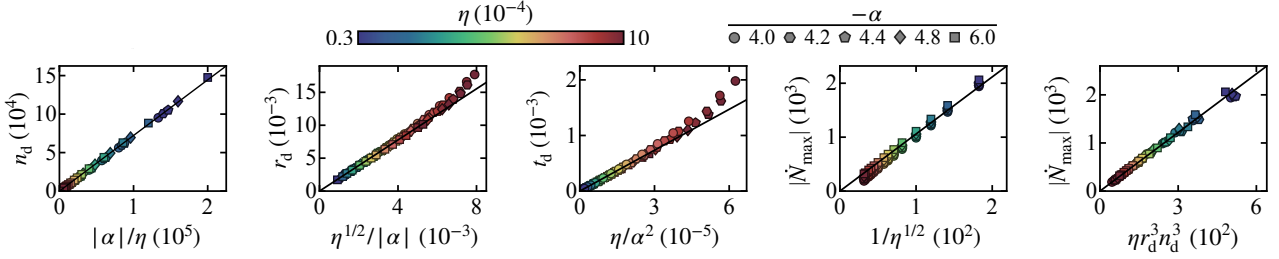


FIG. S3. Testing the Zakharov scaling law predictions (solid lines) for key quantities in our simulations, varying α and η .

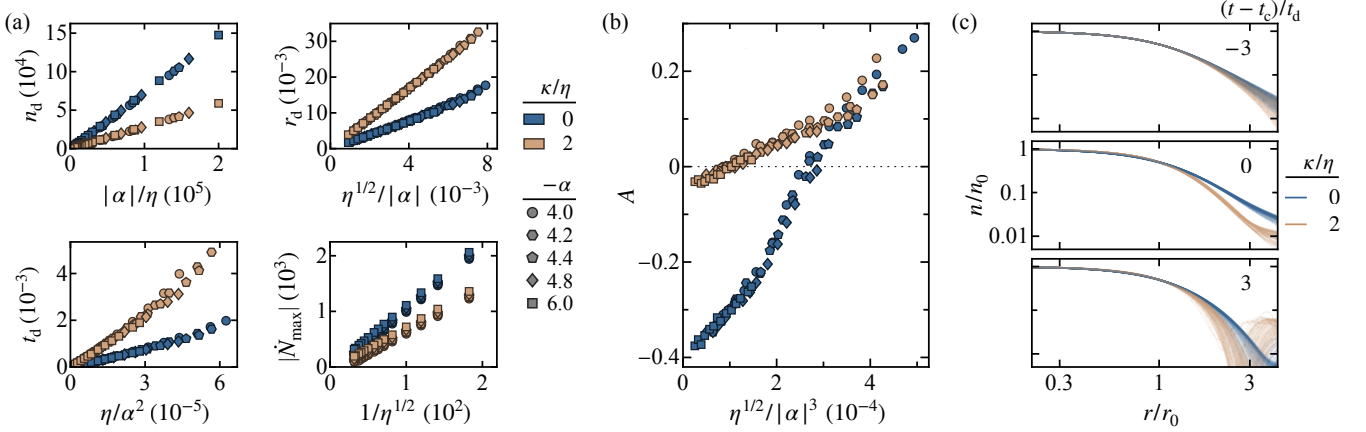


FIG. S4. Additional details on the effects of elastic three-body interactions. (a) The dissipation scales for both $\kappa = 0$ and $\kappa/\eta = 2$, also varying α and η values as in Fig. 4(a). (b) The loss asymmetry A versus $\eta^{1/2}/|\alpha|^3$ for both $\kappa = 0$ and $\kappa/\eta = 2$, varying α and η as in (a). (c) The normalized density profiles at three characteristic $(t - t_c)/t_d$ (panels) for $\kappa = 0$ and $\kappa/\eta = 2$, varying α and η values as in (a).

In Fig. S4, we provide additional details on the effects of elastic three-body interactions, by comparing $\kappa = 0$ and $\kappa/\eta = 2$ for the same α and η values as in Fig. 4(a).

In Fig. S4(a), we show that the Zakharov scaling laws for n_d , r_d , t_d , and \dot{N}_{\max} remain essentially universal for $\kappa/\eta = 2$, while the proportionality constants differ significantly. Qualitatively, one may expect the collapse to be arrested when $n_0 = n_d$ such that $|\alpha|n_d \sim |\kappa - i\eta|n_d^2$, so introducing $\kappa > 0$ decreases n_d , $|\dot{N}_{\max}|$, $1/r_d$, and $1/t_d$. Note that for $\eta = 0$ and $\alpha < 0$, exotic quantum droplets are predicted, where the

repulsive three-body interactions can stabilize the system so long as N is above a critical value $N_c \propto \kappa^{1/2}/\alpha^2$ [45, 46, 71], which may suggest a continuous connection with the scaling $\Delta N \propto \eta^{1/2}/\alpha^2$ for $\kappa = 0$. However, exploring the full dynamical phase diagram deserves a separate dedicated study (see also [71, 72]).

As shown in Fig. S4(b), for $\eta^{1/2}/|\alpha|^3 \rightarrow 0$, $|A|$ is significantly smaller for $\kappa/\eta = 2$, which reflects the suppression of the hotspot behavior. In Fig. 4(c), we plot the normalized density profiles for $\kappa = 0$ and $\kappa/\eta = 2$ at three different $(t - t_c)/t_d$, which show differences for $t \gtrsim t_c$.